ISSN 1674-1056
http://cpb.iphy.ac.cn
http://iopscience.iop.org/cpb
中国物理 B
Chinese Physics
中国物理
Chinese Physics B

Structural and thermal stabilities of Au@Ag core-shell nanoparticles and their arrays: A molecular dynamics simulation

Hai-Hong Jia(贾海洪), De-Liang Bao(包德亮), Yu-Yang Zhang(张余洋), Shi-Xuan Du(杜世萱)
Citation: Chin. Phys. B . 2020, 29(4): 048701 . **doi:** 10.1088/1674-1056/ab7da9
Journal homepage: http://cpb.iphy.ac.cn; http://iopscience.iop.org/cpb

What follows is a list of articles you may be interested in

Unidirectional rotation of circles driven by chiral active particles

Jiamin Chen(陈佳敏), Xiaolin Zhou(周晓琳), Linxi Zhang(章林溪)
Chin. Phys. B . 2018, 27(11): 118701 . **doi:** 10.1088/1674-1056/27/11/118701

Molecular dynamic simulation of the thermodynamic and kinetic properties of nucleotide base pair

Yu-Jie Wang(王宇杰), Zhen Wang(王珍), Yan-Li Wang(王晏莉), Wen-Bing Zhang(张文炳)
Chin. Phys. B . 2017, 26(12): 128705 . **doi:** 10.1088/1674-1056/26/12/128705

Modulation of intra- and inter-sheet interactions in short peptide self-assembly by acetonitrile in aqueous solution

Li Deng(邓礼), Yurong Zhao(赵玉荣), Peng Zhou(周鹏), Hai Xu(徐海), Yanting Wang(王延颋)
Chin. Phys. B . 2016, 25(12): 128704 . **doi:** 10.1088/1674-1056/25/12/128704

Segregations and desorptions of Ge atoms in nanocomposite $Si_{1-x}Ge_x$ films during high-temperature annealing

Yu Wang(汪煜), Meng Yang(杨濛), Gang Wang(王刚), Xiao-Xu Wei(魏晓旭), Jun-Zhuan Wang(王军转), Yun Li(李昀), Ze-Wen Zou(左则文), You-Dou Zheng(郑有炓), Yi Shi(施毅)
Chin. Phys. B . 2017, 26(12): 126801 . **doi:** 10.1088/1674-1056/26/12/126801

Structural and thermal stabilities of Au@Ag core-shell nanoparticles and their arrays: A molecular dynamics simulation*

Hai-Hong Jia(贾海洪)[1,2], De-Liang Bao(包德亮)[1,2], Yu-Yang Zhang(张余洋)[1,2], and Shi-Xuan Du(杜世萱)[1,2,†]

[1] *Institute of Physics, Chinese Academy of Sciences, Beijing* 100190, *China*
[2] *University of Chinese Academy of Sciences, Chinese Academy of Sciences, Beijing* 100190, *China*

(Received 10 February 2020; revised manuscript received 29 February 2020; accepted manuscript online 9 March 2020)

Thermal stability of core-shell nanoparticles (CSNPs) is crucial to their fabrication processes, chemical and physical properties, and applications. Here we systematically investigate the structural and thermal stabilities of single Au@Ag CSNPs with different sizes and their arrays by means of all-atom molecular dynamics simulations. The formation energies of all Au@Ag CSNPs we reported are all negative, indicating that Au@Ag CSNPs are energetically favorable to be formed. For Au@Ag CSNPs with the same core size, their melting points increase with increasing shell thickness. If we keep the shell thickness unchanged, the melting points increase as the core sizes increase except for the CSNP with the smallest core size and a bilayer Ag shell. The melting points of Au@Ag CSNPs show a feature of non-monotonicity with increasing core size at a fixed NP size. Further simulations on the Au@Ag CSNP arrays with 923 atoms reveal that their melting points decrease dramatically compared with single Au@Ag CSNPs. We find that the premelting processes start from the surface region for both the single NPs and their arrays.

Keywords: bimetallic nanoparticles, thermal stability, melting point

PACS: 87.10.Tf, 68.60.Dv **DOI:** 10.1088/1674-1056/ab7da9

1. Introduction

Bimetallic nanoparticles (BNPs), composed of two different metal elements, have attracted great interest due to their novel electronic,[1] optical,[2–4] catalytic[4–7] and photocatalytic[4] properties. Depending on the synthesis procedures, the configuration of BNPs can be alloyed,[8–13] core-shelled,[11,14–16] etc. For the core-shell BNPs (CSNPs), one metal element forms a core and the other forms a concentric shell, while for the alloyed ones, the distribution of the two types of atoms is discrete. Consequently, the properties of BNPs can be tuned not only by varying their sizes and shapes, but also by changing the spatial distribution of two metal elements. CSNPs with different functionalities have been designed by changing the core-to-shell volume ratio.[3,17–20] For example, the efficiency of the catalytic reaction was increased with increasing core size of Au@Ag CSNPs.[19] Through systematic investigation on the localized surface plasmon resonance (LSPR) properties of the Au@Ag core-shell nanotubes as a function of the Ag shell thickness, Ma *et al.* found that a shell thickness of 3 nm completely screened the LSPR of the Au cores.[3] As for bimetallic nanoalloys, numerous works have been devoted to explore highly efficient nanoalloy-based catalysts by tuning component ratios.[21–24] However, high temperature is inevitably involved not only in the synthesis and postprocessing (thermal annealing) processes of BNPs but also in their applications such as high-temperature catalytic reactions. The structural, chemical and physical properties of BNPs can be changed significantly with increasing temperature.[25] In view of this, extensive efforts have been taken to investigation of the thermal stabilities of BNPs in experiments[25–27] and theory.[28–42]

Among a wide range of BNPs, Au–Ag NPs have shown great potential in the field of optics,[2,3,43,44] biosensor[45–47] and catalysis.[48–50] Similar lattice constant and chemical environment in their bulk phase facilitate the synthesis of Au–Ag alloy[51,52] or core-shell[53–55] nanoparticles. The effects of structural factors, such as shape,[56] atomic arrangement[56,57] and component,[57,58] on the thermal stabilities of Au-Ag BNPs have been investigated theoretically by several research groups. Chen *et al.* studied the component effect on the thermal stability of Au_xAg_{55-x} with a fixed size of 55 atoms and found that the melting point decreases with increasing Au concentration.[58] Qi *et al.* found that both the shape and atomic configuration effects are minor factors in affecting the melting temperature of Au–Ag BNPs.[56] The calculated formation energies of NPs with 555 atoms and 959 atoms indicate that the large NPs are more stable than the small ones with the same composition. Gould *et al.* reported that the melting points of Au@Ag CSNPs are much higher than Ag@Au CSNPs with a fixed size of 147 atoms.[57] However, systematically investigating the effects of both the core size and the shell size on the thermal stabilities of Au@Ag CSNPs with different

*Project supported by the National Key Research & Development Project of China (Grant No. 2016YFA0202300), the National Natural Science Foundation of China (Grant No. 61888102), the Strategic Priority Research Program of Chinese Academy of Sciences (Grant No. XDB30000000), and the Beijing Nova Program of China (Grant No. Z181100006218023).

†Corresponding author. E-mail: sxdu@iphy.ac.cn

© 2020 Chinese Physical Society and IOP Publishing Ltd

sizes is still lacking. Moreover, though the NPs synthesized are always assembly structures, the theoretical investigations are mainly focused on a single NP or several NPs with a limited number of NPs. A theoretical study of arrays of NPs is also important to understand the experimental observations.

In this article, we choose small size of NPs to study their structural and thermal stabilities because the NP as a catalyst becomes more effective as its size goes down and its melting point is very different from its bulk. The Au@Ag CSNPs are constructed by doping different numbers of Au atoms into the core of Ag NPs with different sizes and we investigate the effects of both the core and the shell sizes on the thermal stability of these Au@Ag CSNPs. Molecular dynamics (MD) simulations with embedded-atoms method (EAM) potential are used to study the structural and thermal stabilities of Au@Ag CSNPs and close-packed arrays. It is found that for Au@Ag CSNPs with the same core size, the melting points increase with increasing shell thickness. Except for Au@Ag CSNP with 13 Au and 134 Ag atoms, an increase of the thickness of Au core leads to an increase of the melting point when the thickness of Ag shell is fixed. For Au@Ag CSNPs at a fixed size, the melting points show a feature of non-monotonicity with increasing core size, either higher or lower than that of a AgNP with the same size. Furthermore, the thermal stability of a two-dimensional close-packed Au@Ag CSNP (with 923 atoms) array has also been explored. It is found that the thermal stability of a single Au@Ag CSNP is much better than their arrays.

2. Computational methods

2.1. Initial configurations setup

Because the icosahedral motif is the most favored configuration for NPs with less than 3000 atoms,[59,60] here we only consider the stability of icosahedral NPs. For an icosahedron with K atomic layers, the magic number of atoms can be written as

$$N(K) = \frac{10}{3}K^3 - \frac{5}{2}K^2 + \frac{10}{3}K - 1. \quad (1)$$

Therefore, icosahedral Ag NPs with 147 atoms consists of four atomic layers. In this work, icosahedral Ag NPs with four (147 atoms), five (309 atoms), six (561 atoms), and seven (923 atoms) atomic layers are constructed to study the cluster size effect on thermodynamic stability of NPs. For each Ag NP, we dope different layers of Au atoms as a core to study the effects of core size on thermal stability of Au@Ag CSNPs. Since the particles with one layer of Au core only has one atom and their properties are sensitive to the doping environment,[57] we did not include them in our calculation. To differentiate these Au@Ag CSNPs, $Au_x@Ag_{K-x}$ are used, where x is the number of Au layers and K is the total number of layers of the NP. Ag NPs and Au NPs are regarded as special cases of Au@Ag CSNPs, where the thicknesses of the Au core are 0 and K, respectively. The initial configurations of these NPs are shown in Fig. 1.

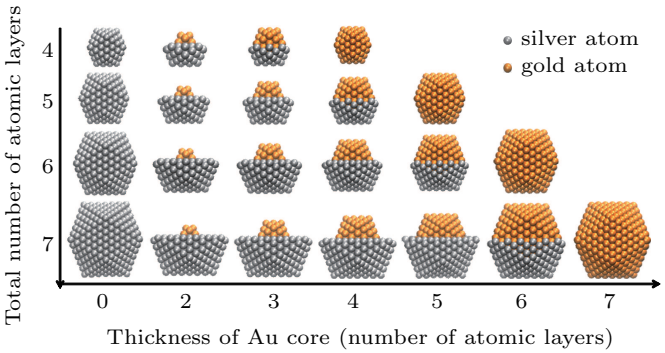


Fig. 1. Schematic diagrams of the atomic arrangement of Ag NPs, Au@Ag CSNPs and Au NPs. To clearly see the size of the Au core, only bottom half of Ag atoms for Au@Ag CSNPs are shown here.

2.2. Potential model

The integrated EAM potential database developed by Zhou *et al.* is applicable to a number of metals and their alloys including Ag, Au and AuAg alloys.[61–64] In the EAM potential model, the total energy of the system is defined as

$$E = \frac{1}{2}\sum_{i,j,i\neq j}\phi_{ij}(r_{ij}) + \sum_i F_i(\rho_i), \quad (2)$$

where ϕ_{ij} represents the pair energy between atoms i and j separated by a distance of r_{ij}, and F_i is the embedding energy associated with embedding an atom i into a local site with an electron density ρ_i. The electron density can be calculated using

$$\rho_i = \sum_{j,j\neq i} f_j(r_{ij}), \quad (3)$$

where $f_j(r_{ij})$ is the electron density at the site of atom i arising from j at a distance of r_{ij} away.

2.3. Simulation details

The software used in our simulation is a large-scale atomic molecular massively parallel simulator (LAMMPS). Upon starting the MD simulations, all NPs are first quasi-statically relaxed to a local minimum energy state through the steepest descent method. All simulations are conducted under the NVT (fixed number of particles, volume, and temperature) ensemble with Nosé–Hoove thermostat with a relaxation time of 0.1 ps. The time step of 2 fs is used. Periodic boundary condition (PBC) is applied in three dimensions. For single NPs, a vacuum layer in simulation cells (>2 nm) is large enough to ignore interactions between neighboring NPs. In order to study the thermal behavior, NPs are heated from 300 K to 1000 K with an interval of 5 K. At each temperature, we heat the sample to the setting temperature in 0.1 ns and do the simulation under NVT for 8 ns to achieve an equilibrium state. The equilibrium state then undergoes a 2 ns production run in which the trajectories are stored every 1 ps.

3. Results and discussion

3.1. Stability of single Au@Ag CSNPs

The stabilities of Au@Ag CSNPs with different sizes at 0 K are investigated by calculating their formation energies. The formation energy E_f is defined as[37,56]

$$E_f = E_{AB} - \chi E_B - (1-\chi) E_A, \tag{4}$$

where E_{AB}, E_A, and E_B are the cohesive energies of bimetallic NP, NPs with pure component A and B, respectively; χ is the atomic concentration. The E_f values for different Au@Ag CSNPs are listed in Table 1.

For an NP with four layers, as shown in Table 1, the mean cohesive energies for pure Ag and Au NPs are −2.45 eV and −3.52 eV, respectively. Both the mean cohesive energies are higher than their corresponding bulk values −2.85 eV and −3.93 eV for Ag and Au, respectively. This suggests that the stability of bulk metal decreases when the size is in nanoscale. With the increasing NP size, the mean cohesive energies for pure Ag and Au NPs decrease, suggesting an increasing stability of pure NPs as the size of the NP increase. In addition, we find that the formation energies of Au@Ag CSNPs are all negative, indicating that Au@Ag CSNPs are energetically favorable to be formed.

3.2. Melting temperature of single Au@Ag CSNPs

To simulate the melting process, we increase the temperature of Au@Ag CSNPs from 300 K to 1000 K with an interval of 5 K. Lindemann index, an effective indicator of the thermally driven disorder, which has been widely applied to determine the melting point (T_m) of NPs,[65] is calculated for each temperature. For a system in which the number of atoms is N, the local Lindemann index of atom i can be defined as

$$q_i = \frac{1}{N-1} \sum_{j \neq i} \frac{\sqrt{\left\langle r_{ij}^2 \right\rangle - \left\langle r_{ij} \right\rangle^2}}{\left\langle r_{ij} \right\rangle}, \tag{5}$$

where angular brackets indicate a time average at a constant temperature. The system-averaged Lindemann index is calculated by $\delta = \frac{1}{N} \sum_i q_i$.

It is generally accepted that a value of δ smaller than ∼0.1 indicates a solid state, while a value larger than ∼0.1 is a liquid state.[66] Here we employ a Lindeman index of 0.1 as the criterion to determine the melting point. These melting points have been further confirmed by using common neighbor analysis. Temperature dependences of the Lindemann indices for Ag NPs, Au NPs, and Au@Ag CSNPs with different sizes are shown in Fig. 2. We find that the Lindemann indices increase linearly at the beginning of heating and show an obvious and nonlinear increase as the temperature is close to the melting point. The solid and liquid phases coexist in the vicinity of the melting point, corresponding to the premelting stage. It is difficult for us to determine the melting point of Au_4 directly by Lindemann index because of the slow solid-liquid deformation, which is similar to the observation of Gould *et al.*[57] Here the Lindemann index in combination with a common neighbor analysis (the next section will describe this parameter in detail) is used to decide the melting point of Au_4. The melting points of Ag NPs, Au NPs, and Au@Ag CSNPs are given in Table 1.

Table 1. The mean cohesive energies per atom (E_{coh}), formation energies (E_f), surface area to volume ratios (sa/vol) and melting points (T_m) of single Au@Ag CSNPs with different sizes.

Composition	Number of atoms in NPs	E_{coh}/eV	E_f/eV	(sa/vol)/Å^{-1}	T_m/K
Ag_4	147	−2.450	0	0.462	835
Au_4	147	−3.522	0	0.470	720
$Au_2@Ag_2$	147	−2.555	−1.500	0.462	875
$Au_3@Ag_1$	147	−2.911	−8.807	0.462	770
Ag_5	309	−2.542	0	0.345	875
Au_5	309	−3.614	0	0.351	855
$Au_2@Ag_3$	309	−2.590	−0.896	0.345	900
$Au_3@Ag_2$	309	−2.741	−2.531	0.345	870
$Au_4@Ag_1$	309	−3.101	−15.147	0.345	820
Ag_6	561	−2.598	0	0.275	900
Au_6	561	−3.671	0	0.280	885
$Au_2@Ag_4$	561	−2.624	−0.637	0.274	915
$Au_3@Ag_3$	561	−2.707	−2.134	0.276	915
$Au_4@Ag_2$	561	−2.887	−4.398	0.275	915
$Au_5@Ag_1$	561	−3.230	−22.995	0.274	860
Ag_7	923	−2.635	0	0.228	960
Au_7	923	−3.708	0	0.230	960
$Au_2@Ag_5$	923	−2.651	−0.819	0.228	945
$Au_3@Ag_4$	923	−2.701	−1.903	0.228	955
$Au_4@Ag_3$	923	−2.811	−4.717	0.228	955
$Au_5@Ag_2$	923	−3.003	−8.107	0.228	960
$Au_6@Ag_1$	923	−3.325	−34.917	0.228	905

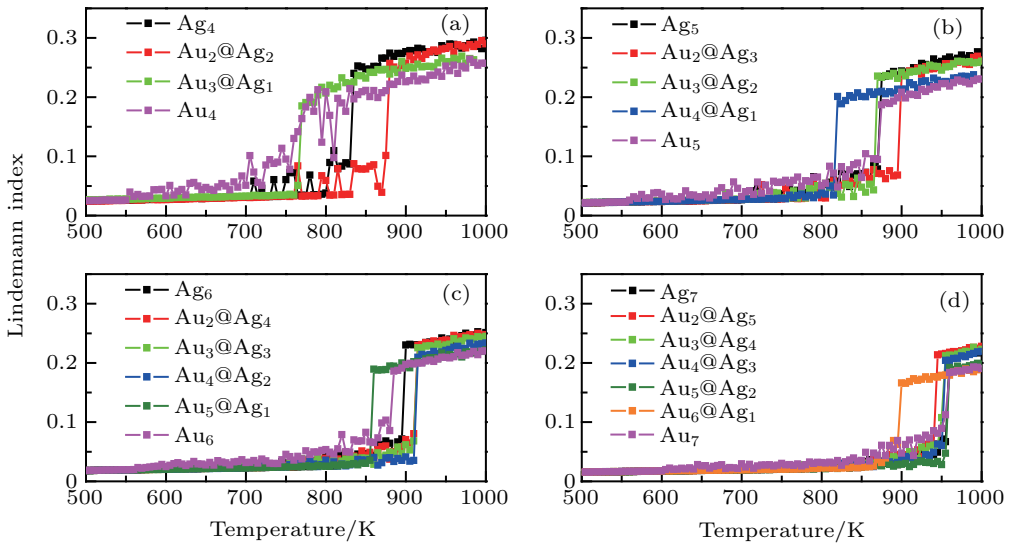


Fig. 2. Lindemann indices as a function of temperature for Ag NPs, Au@Ag CSNPs and Au NPs in different sizes. (a)–(d) Lindemann indices as a function of temperature for NPs with four, five, six and seven atomic layers, respectively. The black and pink curves show the Lindemann indices of Ag NPs and Au NPs, respectively. The Lindemann indices of Au@Ag CSNPs with two, three, four and five layers of Au core are plotted by red, green, blue, olive and orange curves, respectively.

It is found that the melting point of Ag NP increases with increasing size, which follows the Pawlow law[67] and agrees with the existing experiments.[68] The Pawlow law is also suitable for Au NPs. However, different from the bulk phase, where the melting point of bulk Au is higher than that of bulk Ag, the melting points of Au NPs are lower than or equal to that of Ag NPs with the same size. For a single-component bulk material, the melting point is proportional to its cohesive energy, according to Lindemann's criterion.[69] The cohesive energy of bulk Ag is -2.85 eV per atom, which is higher than that of bulk Au, -3.93 eV per atom. Therefore, the melting point of bulk Au (1415 K) is higher than that of bulk Ag (1175 K). When bulk material changes to nanoparticles, the melting point decreases because surface atoms with low coordination numbers and greater degrees of freedom have less stability than atoms in the bulk. It is for this reason that the melting process of the monometallic NP begins at surface region, causing the phenomenon of surface premelting.[70] Figure 2 shows that the Lindemann indices of Au NPs (the pink curves) start to fluctuate, indicating a premelting, at lower temperatures than Ag NPs (black curves). The lower premelting temperature of Au NPs is mainly attributed to the higher surface energy of Au (1.5 J·m^{-2}) compared with Ag (1.25 J·m^{-2}).[71] As shown in Table 1, the surface area to volume ratio (sa/vol) of the NP increases with a decreasing NP's size. For a small NP, surface atoms even dominate the melting point. Thus, it is quite possible that the melting point of Au_K ($K = 4$–6) is lower than that of Ag_K ($K = 4$–6) due to the large sa/vol.

Different from the case of NPs composed of single elements, the thermal stability of CSNPs is more complicated due to the versatile atomic arrangement. The melting points of Au@Ag CSNPs with the same core size increase as the shell thickness increases as indicated by the green arrows in Fig. 3(a). The melting points of CSNPs with the same shell thickness increase as the core size increases except for the NPs with a shell thickness of bilayer Ag, as shown in Fig. 3(b). For Au@Ag CSNPs with the same size, the melting points display a feature of non-monotonicity with the increasing thickness of Au core. For Ag NPs with a total layer less than seven, doping Au core with two atomic layers will improve their thermal stabilities.

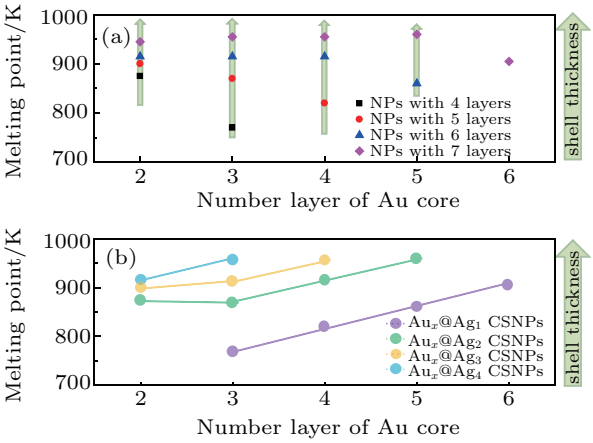


Fig. 3. The melting points of Au@Ag CSNPs with different sizes. (a) The green arrows show that the melting points increase as the shell-size increases with a fixed core size for all the NPs. (b) The dotted lines show that the melting points increase as the core size increases with a fixed shell thickness for all the NPs except for the $Au_2@Ag_2$ CSNP.

3.3. Structural evolution of single Au@Ag CSNPs during the melting process

To investigate the structural changes of BNPs during melting process, the radial distribution functions (RDF) are calculated at the initial temperature of 300 K and at the melting point. The RDFs of Ag NPs, Au NPs and $Au_2@Ag_{K-2}$ CSNPs ($K = 4$–7, four different sizes) at 300 K and their melting points are shown in Figs. 4(a)–4(d). For Au@Ag CSNPs

in each size, only one typical core-to-shell ratio is given here because the other CSNPs with the same particle radius are very similar to the given ones. There are many RDF peaks at 300 K (black curves in each panel) for all the simulated NPs, indicating that the atomic structure is long-range ordered in each case. At melting point, the RDF peaks (red curves) become broader and the height of RDF peaks become lower. In addition, many characteristic peaks disappear, indicating the decrease of structural order.

In order to monitor the structural evolution of Au@Ag CSNPs during heating, we applied the common neighbor analysis (CNA)[72] for all the NPs to investigate the local order of the NPs. In the CNA method, each bond that connects a central atom and its nearby neighbors is characterized by a set of four characteristic numbers, i, j, k, and l. These numbers depend on whether the atoms are nearest (1) or next-nearest (2) neighbors (i), the number of nearest neighbors that they have in common (j), the number of bonds among these common neighbors (k), and the number of bonds in the longest continuous chain of bonds connecting the common neighbors (l). For example, an atom located in a face-centered cubic (fcc) environment forms 12 pairs of 1421 type bonds with its nearest neighbors. For an atom located in a hexagonal close packing (hcp) environment, it forms 6 pairs of 1421 type and 6 pairs of 1422 type bonds with its nearest neighbors. Based on CNA, each atom in an NP can be classified according to its local crystal structure. In this work, the atoms in NPs are classified into four categories: atoms in a local hcp, fcc and icosahedral order are classified as hcp, fcc and ico atoms, respectively; atoms in all other local orders are collectively considered to be "other" atoms because they do not reveal any usefully structural information. We have presented the percentage of the hcp, ico and other coordination atoms as a function of temperature for Ag NPs, Au NPs and $Au_2@Ag_{K-2}$ CSNPs ($K = 4$–7) in Fig. 5. At temperature below 500 K, the percentage of the three types of atoms remain unchanged. By increasing the temperature, a sudden increase of other atoms and a decrease of ico, fcc and hcp atoms to 0% indicates a transition from crystalline structure to amorphous one, suggesting the melting of the NPs.

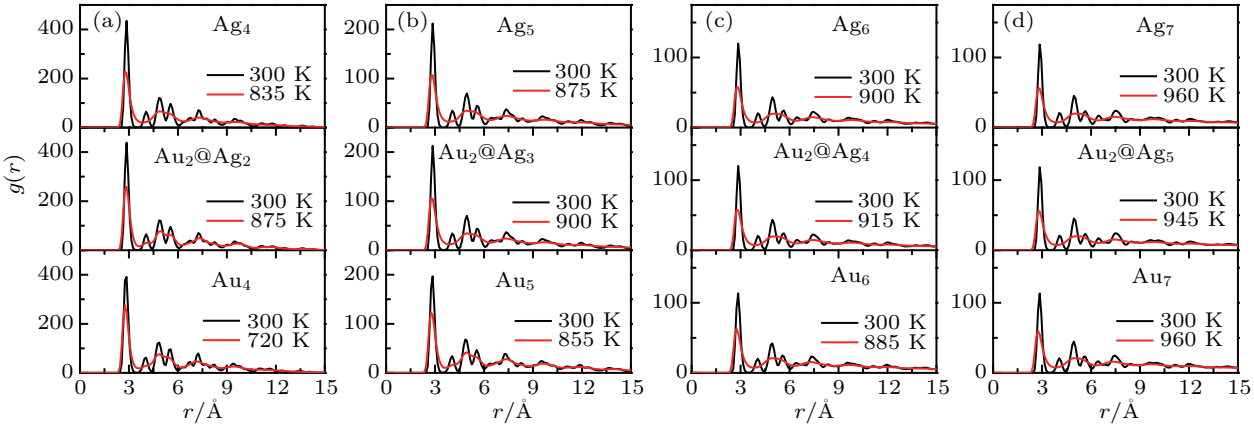


Fig. 4. Radial distribution function in single Ag_K NPs, $Au_2@Ag_{K-2}$ CSNPs, and Au_K NPs at 300 K and their melting temperatures, $K = 4$ (a), 5 (b), 6 (c), 7 (d).

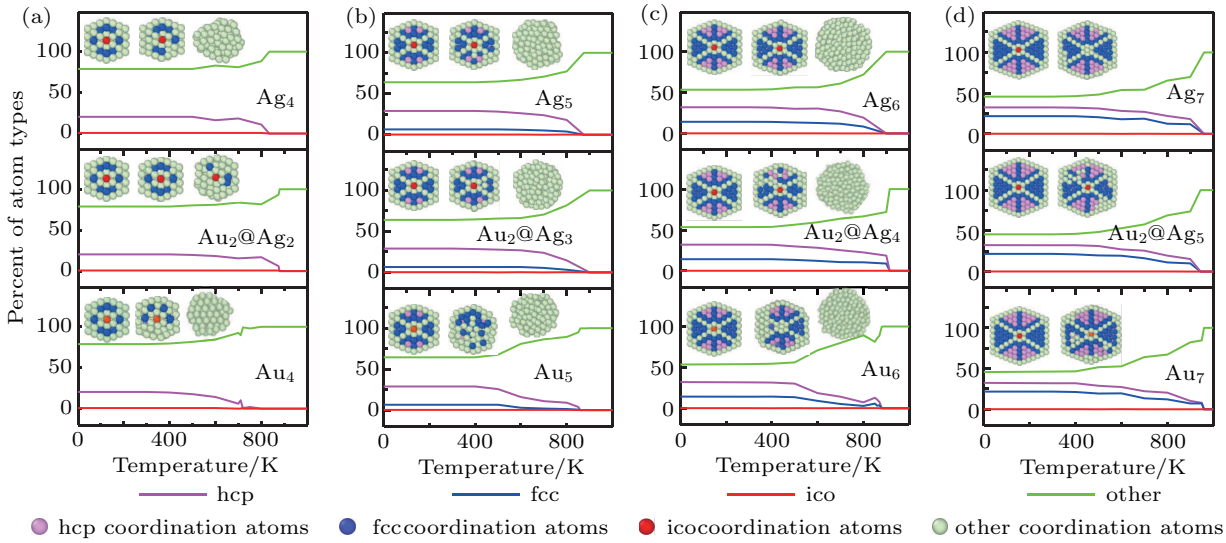


Fig. 5. Percentage of the hcp, ico and other coordination atoms as a function of temperature. (a) $Au_x@Ag_{4-x}$, (b) $Au_x@Ag_{5-x}$, (c) $Au_x@Ag_{6-x}$, (d) $Au_x@Ag_{7-x}$. The insets are the corresponding snapshots of cross sections of nanoparticles. The snapshots are the structure at 0 K, 600 K and the melting temperature from left to right, respectively.

Figure 6(a) shows the cross sections of snapshots of $Au_x@Ag_{7-x}$ ($x = 0$, 2, 7) at melting temperature and several temperatures before melting. We find that the surface atoms start melting at around 800 K while the inside atoms keep the crystalline configuration. This premelting behavior exists in both CSNPs and pure Ag/Au nanoparticles. At a temperature higher than 800 K, the disordering of the NPs extends from the surface to the core gradually. At melting temperature, the disordering of the NP results in a transformation from crystalline structures to amorphous ones. The similar melting behavior is also observed in $Au_3@Ag_4$, $Au_4@Ag_3$, $Au_5@Ag_2$, and $Au_6@Ag_1$ CSNPs. For small NPs, the premelting process also starts from the surface, and gradually extends to the core. Thus, we only show one typical composition for each size of NPs in Fig. 6(b). For $Au_2@Ag_{K-2}$, it is obvious that more atoms in the thicker-shell CSNPs keep the crystalline structure at 800 K than those in the thinner-shell CSNPs, implying an increase of thermal stability with increasing thickness of Ag shell of Au@Ag CSNP with fixed Au core. This finding is in agreement with the results in Fig. 2.

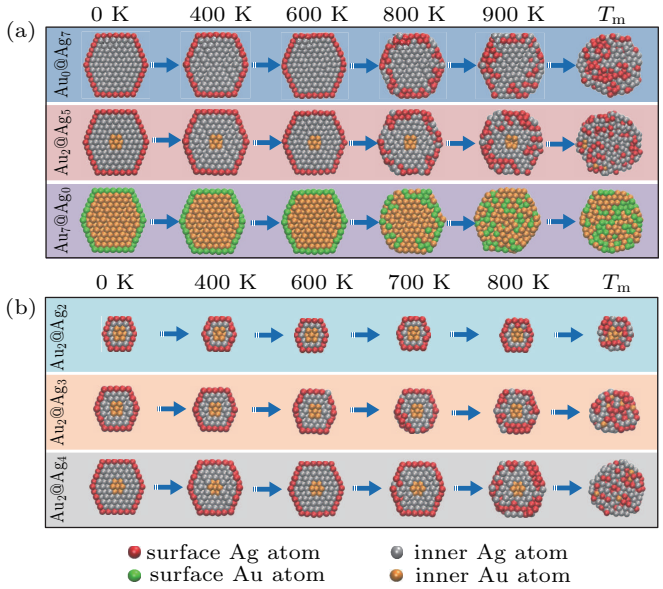


Fig. 6. Snapshots of cross section of NPs at different temperatures during heating process. (a) $Au_x@Ag_{7-x}$ ($x = 0$, 2, 7 are shown in top, middle and bottom panel, respectively), (b) $Au_2@Ag_{K-2}$ ($K = 4$–6 are shown in top, middle and bottom panel, respectively).

3.4. Thermal stability and melting behavior of $Au_x@Ag_{7-x}$ CSNP arrays

A two-dimensional (2D) ordered array of Au–Ag BNPs has been used as plasmonic substrate to improve the sensitivity of surface-enhanced Raman spectroscopy.[73–77] It is expected that the thermal stability and melting behavior of the Au-Ag BNP array are different from their single NPs. In previous work, the two- or three-NP sintering model has been extensively used to study the sintering process of loosely packed NPs.[78–80] While for a closed-packed NP array, such sintering models overlook the pore effect, which significantly contributes to the porosity of final sintered structures.[81,82] Therefore, a simulation based on a real case, 2D array, is essential for elucidating the sintering mechanism of closed-packed NP array.

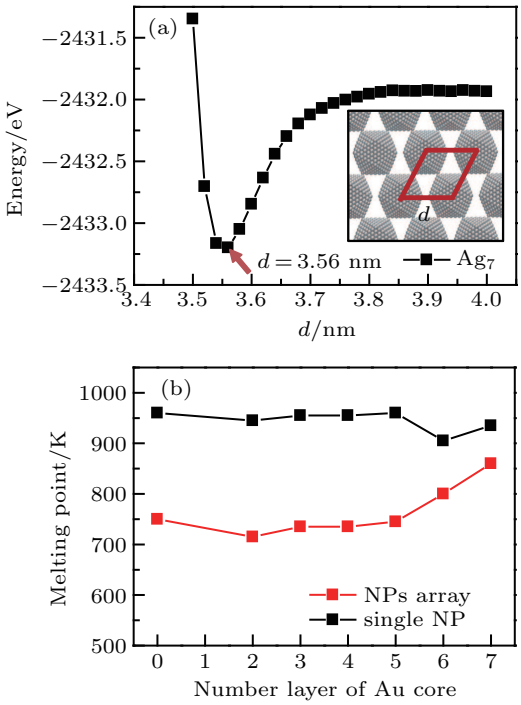


Fig. 7. Energy evolution of Ag_7 NP array and the melting points of single $Au_x@Ag_{7-x}$ NPs and arrays. (a) The total energy per unit cell of Ag_7 NP array as a function of the distance between two neighboring NPs. The unit cell with the lowest energy for Ag_7 is the one in which $d = 3.56$ nm. Inset shows the configuration of a Ag_7 NP array and the unit cell (red rhombus). (b) Composition-dependent melting points of $Au_x@Ag_{7-x}$ NP arrays (red) and the corresponding single $Au_x@Ag_{7-x}$ NPs (black).

We use $Au_x@Ag_{7-x}$ CSNPs containing 923 atoms to set up an NP array and investigate the effect of the core-to-shell ratio on the thermal stability and melting behavior of the NP array. Close-packed NP arrays are energy favorable for hard NPs.[83] To determine the lattice constant of close-packed $Au_x@Ag_{7-x}$ NP arrays, we calculate the total energy per unit cell as a function of the distance between the center of mass of neighboring NPs. It is found that the lattice constants are all around 3.56 nm for $Au_x@Ag_{7-x}$ ($x = 0$, 2–7) NPs arrays. The result of Ag_7 NP arrays is shown in Fig. 7(a) as an example. Then, the arrays are heated from 300 K to 1000 K with a step of 5 K. By analyzing the Lindemann index for these NP arrays as a function of temperature, the melting points are 745 K, 715 K, 735 K, 735 K, 745 K, 800 K, and 860 K for $Au_x@Ag_{7-x}$ ($x = 0$, 2–7), respectively. The melting temperatures of NP arrays are much lower than those of the corresponding single NPs, as shown in Fig. 7(b), because an NP tends to coalesce with its neighbors to decrease the surface energy. Therefore, the Lindemann index reaches the criteria of melting point at lower temperatures in comparison with single NPs.

Figure 8 shows the top view of snapshots and cross sections for Ag_7, $Au_2@Ag_5$ and Au_7 CSNP arrays at their melting temperatures and at four different temperatures before melting. We find that the melting starts from the surface, which is similar to the single NPs. The NP array transforms to a continuing film at melting temperature where the surface energy decreases as their surface areas decrease. For Ag_7 NP and $Au_2@Ag_5$ CSNP arrays, different from the single NPs which involve a gradually melting from the surface to the core, the NP arrays directly transform to a film after premelting of surface layers. The melting behavior of other $Au_x@Ag_{7-x}$ CSNP arrays are similar to that of $Au_2@Ag_5$ CSNP arrays. For a Au_7 NP array, the spaces between NPs disappear at 550 K with a corrugated surface, which is different from Ag NP and Au@Ag CSNP arrays. As the temperature increases, the corrugated surface gradually changes to a flat one at 860 K.

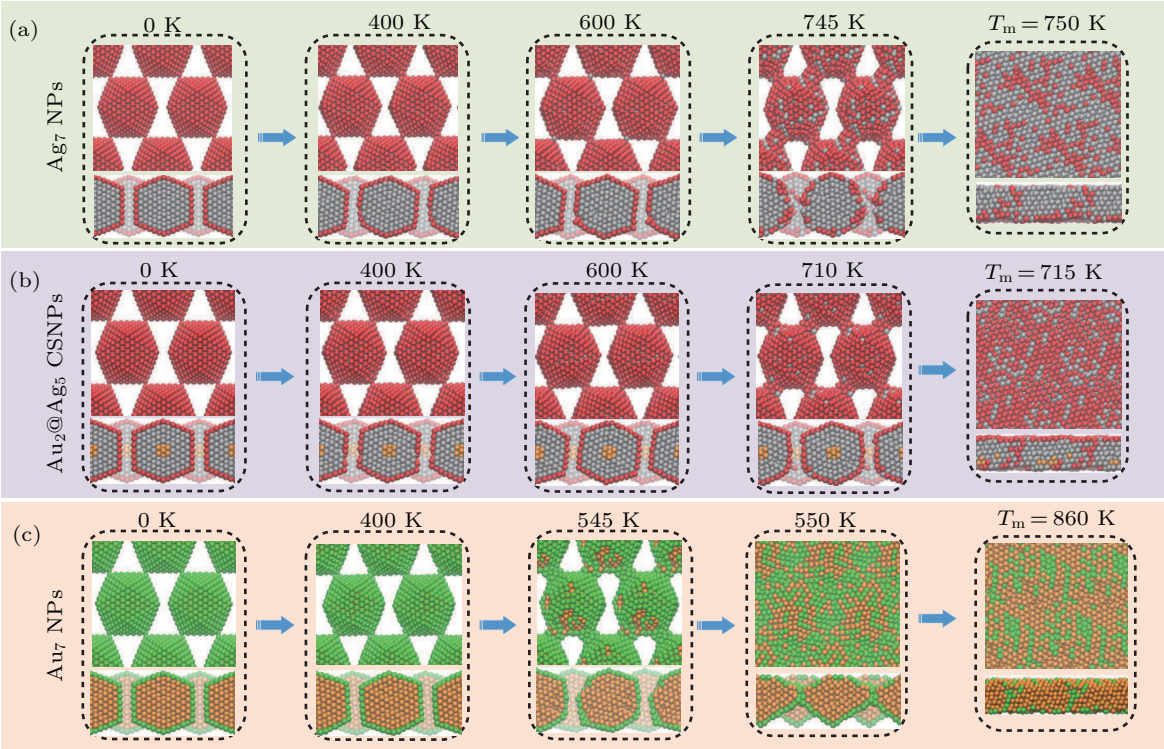


Fig. 8. Snapshots of cross section of Ag NP, Au@Ag CSNP and Au NP arrays at different temperatures during heating process. (a) Ag_7 NP array, (b) $Au_2@Ag_5$ CSNP array, (c) Au_7 NP array. The upper panels are top views, the lower panels are cross sections. Surface Ag, inner Ag, surface Au and inner Au atoms are marked by red, silver, green and orange, respectively.

4. Conclusion and perspectives

In this study, the effects of core and shell sizes on the thermal stability of Au@Ag CSNPs with varying particle radius are investigated by MD simulations. For Au@Ag CSNPs, an increase of the thickness of Ag shell leads to an increase of the melting point when the thickness of Au core is unchanged. Except for $Au_2@Ag_2$ CSNPs, the melting point of Au@Ag CSNP increases as the thickness of Au core increases with a fixed thickness of Ag shell. For Au@Ag CSNPs with the same size, the melting points display a feature of non-monotonicity with the increasing core-to-shell ratio. For all these BNPs, the premelting process starts from the surface, and gradually extends to the interior. In addition, we have studied the thermal stability and melting behavior of $Au_x@Ag_{7-x}$ CSNP array. It is found that the melting point of $Au_x@Ag_{7-x}$ CSNP array is much lower than the corresponding single NP. The premelting of $Au_x@Ag_{7-x}$ CSNP array also starts from the shell region. When reaching the melting point, icosahedral NP transforms into a continuing layer. These results provide a better understanding of thermal stability of Au@Ag CSNPs (their array) and are expected to be useful for the construction and production of BNP with special stability.

Acknowledgments

We thank professor Min Ouyang for constructive discussions and suggestions. MD simulations were carried out on TianHe-1A at the National Supercomputer Center in Tianjin.

References

[1] Strasser P, Koh S, Anniyev T, Greeley J, More K, Yu C, Liu Z, Kaya S, Nordlund D, Ogasawara H, Toney M F and Nilsson A 2010 *Nat. Chem.* **2** 454
[2] Jia X, Li J, Zhang X and Wang E 2015 *Chem. Commun.* **51** 17417
[3] Ma Y, Li W, Cho E C, Li Z, Yu T, Zeng J, Xie Z and Xia Y 2010 *ACS Nano* **4** 6725
[4] Zaleska-Medynska A, Marchelek M, Diak M and Grabowska E 2016 *Adv. Colloid Interface Sci.* **229** 80
[5] Chong L, Wen J, Kubal J, Sen F G, Zou J, Greeley J, Chan M, Barkholtz H, Ding W and Liu D J 2018 *Science* **362** 1276

[6] Fang H, Yang J, Wen M and Wu Q 2018 *Adv. Mater.* **30** 1705698
[7] Jiang H L, Akita T, Ishida T, Haruta M and Xu Q 2011 *J. Am. Chem. Soc.* **133** 1304
[8] Ding K, Cullen D A, Zhang L, Cao Z, Roy A D, Ivanov I N and Cao D 2018 *Science* **362** 560
[9] Wong A, Liu Q, Griffin S, Nicholls A and Regalbuto J R 2017 *Science* **358** 1427
[10] Yao Y, Huang Z, Xie P, Lacey S D, Jacob R J, Xie H, Chen F, Nie A, Pu T, Rehwoldt M, Yu D, Zachariah M R, Wang C, Shahbazian-Yassar R, Li J and Hu L 2018 *Science* **359** 1489
[11] Zhou M, Wang H, Vara M, Hood Z D, Luo M, Yang T H, Bao S, Chi M, Xiao P, Zhang Y and Xia Y 2016 *J. Am. Chem. Soc.* **138** 12263
[12] Ren G, Shi H and Xing Y 2007 *Nanotechnology* **18** 385604
[13] Xiao H J, Shen C M, Shi X Z, Yang S D, Tian Y, Lin S X and Gao H J 2015 *Chin. Phys. B* **24** 078109
[14] Hutzler A, Schmutzler T, Jank M P M, Branscheid R, Unruh T, Spiecker E and Frey L 2018 *Nano Lett.* **18** 7222
[15] Aslam U and Linic S 2017 *ACS Appl. Mater. Interfaces* **9** 43127
[16] Kim T G, Park H J, Woo K, Jeong S, Choi Y and Lee S Y 2018 *ACS Appl. Mater. Interfaces* **10** 1059
[17] Liu K K, Tadepalli S, Tian L and Singamaneni S 2015 *Chem. Mater.* **27** 5261
[18] Moseley P and Curtin W A 2015 *Nano Lett.* **15** 4089
[19] Haldar K K, Kundu S and Patra A 2014 *ACS Appl. Mater. Interfaces* **6** 21946
[20] Binns C, Qureshi M T, Peddis D, Baker S H, Howes P B, Boatwright A, Cavill S A, Dhesi S S, Lari L, Kroger R and Langridge S 2013 *Nano Lett.* **13** 3334
[21] Seraj S, Kunal P, Li H, Henkelman G, Humphrey S M and Werth C J 2017 *ACS Catal.* **7** 3268
[22] Kim S M, Abdala P M, Margossian T, Hosseini D, Foppa L, Armutlulu A, van Beek W, Comas-Vives A, Coperet C and Muller C 2017 *J. Am. Chem. Soc.* **139** 1937
[23] Luo L, Duan Z, Li H, Kim J, Henkelman G and Crooks R M 2017 *J. Am. Chem. Soc.* **139** 5538
[24] García S, Zhang L, Piburn G W, Henkelman G and Humphrey S M 2014 *ACS Nano* **8** 11512
[25] Schnedlitz M, Lasserus M, Meyer R, Knez D, Hofer F, Ernst W E and Hauser A W 2018 *Chem. Mater.* **30** 1113
[26] Bonifacio C S, Carenco S, Wu C H, House S D, Bluhm H and Yang J C 2015 *Chem. Mater.* **27** 6960
[27] Vara M, Roling L T, Wang X, Elnabawy A O, Hood Z D, Chi M, Mavrikakis M and Xia Y 2017 *ACS Nano* **11** 4571
[28] Akbarzadeh H, Mehrjouei E, Ramezanzadeh S and Izanloo C 2017 *J. Mol. Liq.* **248** 1078
[29] Akbarzadeh H, Mehrjouei E, Masoumi A and Sokhanvaran V 2018 *J. Mol. Liq.* **249** 477
[30] Huang R, Shao G F, Zhang Y and Wen Y H 2017 *ACS Appl. Mater. Interfaces* **9** 12486
[31] Li M and Cheng D 2013 *J. Phys. Chem. C* **117** 18746
[32] Akbarzadeh H, Abbaspour M and Mehrjouei E 2016 *Phys. Chem. Phys. Chem.* **18** 25676
[33] Akbarzadeh H, Abbaspour M and Mehrjouei E 2017 *J. Mol. Liq.* **242** 1002
[34] Fernández-Navarro C and Mejía-Rosales S 2017 *J. Phys. Chem. C* **121** 21658
[35] Akbarzadeh H, Mehrjouei E and Shamkhali A N 2017 *J. Chem. Phys. Lett.* **8** 2990
[36] Wen Y H, Huang R, Li C, Zhu Z Z and Sun S G 2012 *J. Mater. Chem.* **22** 7380
[37] Huang R, Wen Y H, Zhu Z Z and Sun S G 2016 *Phys. Chem. Phys. Chem.* **18** 9847
[38] Huang R, Wen Y H, Zhu Z Z and Sun S G 2012 *J. Phys. Chem. C* **116** 11837
[39] Huang R, Wen Y H, Shao G F and Sun S G 2013 *J. Phys. Chem. C* **117** 4278
[40] Huang R, Wen Y H, Shao G F, Zhu Z Z and Sun S G 2013 *J. Phys. Chem. C* **117** 6896
[41] Yang Z, Yang X and Xu Z 2008 *J. Phys. Chem. C* **112** 4937
[42] Zhang J P, Zhang Y Y, Wang E P, Tang C M, Cheng X L and Zhang Q H 2016 *Chin. Phys. B* **25** 036102
[43] Rodríguez-González B, Burrows A, Watanabe M, Kiely C J and Liz Marzán L M 2005 *J. Mater. Chem.* **15** 1755
[44] López Lozano X, Mottet C and Weissker H C 2013 *J. Phys. Chem. C* **117** 3062
[45] Mao K, Yang Z, Li J, Zhou X, Li X and Hu J 2017 *Talanta* **175** 338
[46] Mao K, Zhou Z, Han S, Zhou X, Hu J, Li X and Yang Z 2018 *Talanta* **190** 263
[47] Song L, Mao K, Zhou X and Hu J 2016 *Talanta* **146** 285
[48] Wang A Q, Chang C M and Mou C Y 2005 *J. Phys. Chem. B* **109** 18860
[49] Yen C W, Lin M L, Wang A, Chen S A, Chen J M and Mou C Y 2009 *J. Phys. Chem. C* **113** 17831
[50] Slater T J A, Macedo A, Schroeder S L M, Burke M G, O'Brien P, Camargo P H C and Haigh S J 2014 *Nano Lett.* **14** 1921
[51] Liu S, Chen G, Prasad P N and Swihart M T 2011 *Chem. Mater.* **23** 4098
[52] Senapati S, Ahmad A, Khan M I, Sastry M and Kumar R 2005 *Small* **1** 517
[53] Huang Z, Meng G, Hu X, Pan Q, Huo D, Zhou H, Ke Y and Wu N 2019 *Nano Res.* **12** 449
[54] Samal A K, Polavarapu L, Rodal-Cedeira S, Liz-Marzán L M, Pérez-Juste J and Pastoriza-Santos I 2013 *Langmuir* **29** 15076
[55] Yang Y, Shi J, Kawamura G and Nogami M 2008 *Scr. Mater.* **58** 862
[56] Qi W H and Lee S T 2010 *J. Phys. Chem. C* **114** 9580
[57] Gould A L, Logsdail A J and Catlow C R A 2015 *J. Phys. Chem. C* **119** 23685
[58] Chen, Curley B C, Rossi G and Johnston R L 2007 *J. Phys. Chem. C* **111** 9157
[59] Baletto F and Ferrando R 2005 *Rev. Mod. Phys.* **77** 371
[60] Wang B, Liu M, Wang Y and Chen X 2011 *J. Phys. Chem. C* **115** 11374
[61] Zhou X W, Johnson R A and Wadley H N G 2004 *Phys. Rev. B* **69** 144113
[62] Bon M, Ahmad N, Erni R and Passerone D 2019 *J. Chem. Phys.* **151** 064105
[63] Li X G, Hu C Z, Chen C, Deng Z, Luo J and Ong S P 2018 *Phys. Rev. B* **98** 094104
[64] Zhou J, Yang Y, Yang Y, Kim D S, Yuan A, Tian X, Ophus C, Sun F, Schmid A K, Nathanson M, Heinz H, An Q, Zeng H, Ercius P and Miao J 2019 *Nature* **570** 500
[65] Löwen H 1994 *Phys. Rep.* **237** 249
[66] Hansen K 2013 *Statistical Physics of Nanoparticles in the Gas Phase* (The Netherlands: Springer)
[67] Pawlow P 1969 *Z. Phys. Chem.* **65** 1
[68] Asoro M, Damiano J and Ferreira P J 2009 *Microsc. Microanal.* **15** 706
[69] Nanda K K, Sahu S N and Behera S N 2002 *Phys. Rev. A* **66** 013208
[70] Liu X, Wen X and Hoffmann R 2018 *ACS Catal.* **8** 3365
[71] Skriver H L and Rosengaard N M 1992 *Phys. Rev. B* **46** 7157
[72] Honeycutt J D and Andersen H C 1987 *J. Phys. Chem.* **91** 4950
[73] Duan B, Zhou J, Fang Z, Wang C, Wang X, Hemond H F, Chan-Park M B and Duan H 2015 *Nanoscale* **7** 12606
[74] Karn-orachai K, Sakamoto K, Laocharoensuk R, Bamrungsap S, Dharakul T and Miki K 2017 *RSC Adv.* **7** 14099
[75] Karn-orachai K, Sakamoto K, Laocharoensuk R, Bamrungsap S, Songsivilai S, Dharakul T and Miki K 2016 *RSC Adv.* **6** 97791
[76] Pincella F, Song Y, Ochiai T, Isozaki K, Sakamoto K and Miki K 2014 *Chem. Phys. Lett.* **605–606** 115
[77] Zhang P, Yang S, Wang L, Zhao J, Zhu Z, Liu B, Zhong J and Sun X 2014 *Nanotechnology* **25** 245301
[78] Lewis L J, Jensen P and Barrat J L 1997 *Phys. Rev. B* **56** 2248
[79] Jin B, Sushko M L, Liu Z, Jin C and Tang R 2018 *Nano Lett.* **18** 6551
[80] Wang J, Chen S, Cui K, Li D and Chen D 2016 *ACS Nano* **10** 2893
[81] Wang J and Shin S 2017 *RSC Adv.* **7** 21607
[82] Nakao K, Ishimoto T and Koyama M 2014 *J. Phys. Chem. C* **118** 15766
[83] Boles M A, Engel M and Talapin D V 2016 *Chem. Rev.* **116** 11220